Selected for a Viewpoint in *Physics*

RAPID COMMUNICATIONS

PHYSICAL REVIEW B **81**, 041401(R) (2010)

Many-body instability of Coulomb interacting bilayer graphene: Renormalization group approach

Oskar Vafek and Kun Yang

National High Magnetic Field Laboratory and Department of Physics, Florida State University, Tallahassee, Florida 32306, USA

(Received 18 June 2009; revised manuscript received 21 October 2009; published 4 January 2010)

Low-energy electronic structure of (unbiased and undoped) bilayer graphene consists of two Fermi points with *quadratic* dispersions if trigonal warping is ignored. We show that short-range (or screened Coulomb) interactions are marginally *relevant* and use renormalization group to study their effects on low-energy properties of the system. We find that the two quadratic Fermi points spontaneously split into four Dirac points. This results in a nematic state that spontaneously breaks the sixfold lattice rotation symmetry (combined with layer permutation) down to a twofold one, with a finite transition temperature. Critical properties of the transition and effects of trigonal warping are also discussed.

DOI: 10.1103/PhysRevB.81.041401 PACS number(s): 71.10.−w, 71.45.−d

This Rapid Communication is motivated by the observation that in noninteracting systems with susceptibilities diverging as the temperature approaches zero, the inclusion of arbitrarily small interaction leads to a finite but also arbitrarily small transition temperature into an ordered state. The analytical method of choice in this case is the renormalization group (RG), which has the virtue of unbiased determination of the leading instability.[1] Here we apply the RG method to the bilayer graphene with *A-B* stacking.[2–5] While in general, the motion of the noninteracting electrons in such potential does not lead to diverging susceptibilities due to trigonal warping,[3,4] if only nearest-neighbor (nn) hopping is considered each set of four Dirac points merges into a single degenerate point with parabolic dispersion (see Fig. 1). As the nearest-neighbor hopping amplitudes are the largest, the latter is the natural starting point of theoretical analysis.[6,7] The finite density of states associated with the parabolic dispersion leads to screening that renders Coulomb interaction short ranged and to diverging susceptibilities in several channels. We find that the leading instability triggered by the run-away RG flow is in the nematic channel, which effectively makes hopping amplitudes stronger along preferred direction [see Eqs. (17) and (18)], and leads to *spontaneous* splittings of the Fermi points and breaking of the lattice rotation symmetry. Among other effects, this should lead to anisotropic transport in sufficiently clean samples, as well as suppression of the low-energy density of state: an effect, in principle, observable in STM.

We start with the tight-binding Hamiltonian for electrons hopping on the bilayer honeycomb lattice with Bernal stacking

$$\mathcal{H} = \sum_{\langle \mathbf{r}\mathbf{r}'\rangle} [t_{\mathbf{r}\mathbf{r}'} c_\sigma^\dagger(\mathbf{r}) c_\sigma(\mathbf{r}') + \text{H.c.}] + \frac{1}{2}\sum_{\mathbf{r}\mathbf{r}'} \delta\hat{n}(\mathbf{r}) V(\mathbf{r}-\mathbf{r}') \delta\hat{n}(\mathbf{r}'), \tag{1}$$

where, in the nn approximation, the (real) hopping amplitudes t connect the in-plane nn sites belonging to different sublattices and, for one of the sublattices, also the sites vertically above it with amplitude $t_\perp$. Since there are four sites in the unit cell, there are four bands whose dispersion for the above model comes from the solution of the eigenvalue problem,

$$\begin{bmatrix} 0 & d_{\mathbf{k}}^* & t_\perp & 0 \\ d_{\mathbf{k}} & 0 & 0 & 0 \\ t_\perp & 0 & 0 & d_{\mathbf{k}} \\ 0 & 0 & d_{\mathbf{k}}^* & 0 \end{bmatrix} \begin{bmatrix} b_1(\mathbf{k}) \\ a_1(\mathbf{k}) \\ a_2(\mathbf{k}) \\ b_2(\mathbf{k}) \end{bmatrix} = E(\mathbf{k}) \begin{bmatrix} b_1(\mathbf{k}) \\ a_1(\mathbf{k}) \\ a_2(\mathbf{k}) \\ b_2(\mathbf{k}) \end{bmatrix}. \tag{2}$$

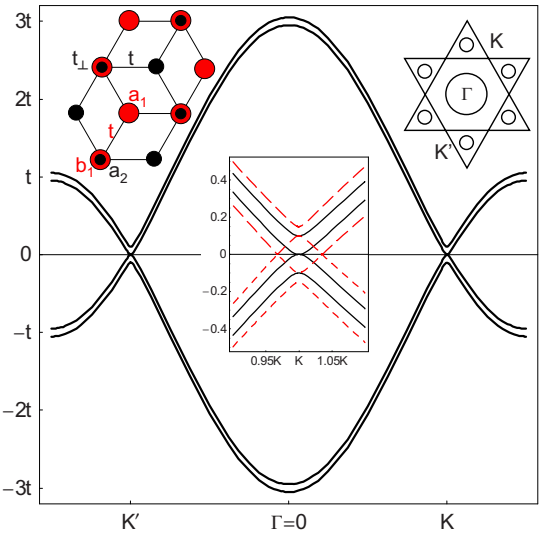

FIG. 1. (Color online) (Upper left inset) Honeycomb bilayer unit cell. Atoms in the lower layer (2) are marked as smaller (black) circles; atoms in the upper layer (1) are larger (red) circles. As a starting point, only the intralayer nearest-neighbor hopping amplitudes t and the interlayer hopping amplitudes $t_\perp$ are considered. (Upper right inset) Schematic constant energy contours of the resulting dispersion. (Main figure) The energy dispersion of the four bands along the vertical cut in the Brillouin zone. The band splitting at the K (and K') points is $t_\perp$. (Middle inset) Magnification of the dispersion (in units of t) near the degeneracy point (solid black) as well as the dispersion in the nematic state (dashed red) with $\Delta_x \neq 0$ [see Eq. (17)].

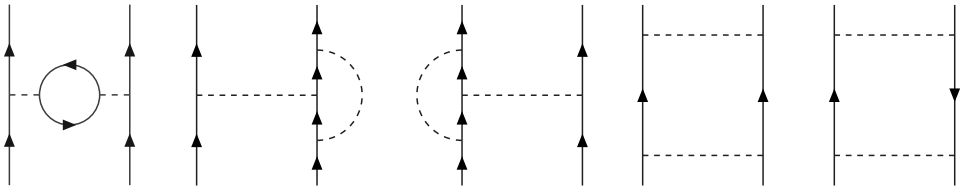

FIG. 2. Diagrams appearing at one-loop RG. The vertices are either $\delta_{\alpha\beta}$ or $\Sigma^{\mu}_{\alpha\beta}$.

We find $E(\mathbf{k})=\pm(\frac{1}{2}t_{\perp}\pm\sqrt{|d_{\mathbf{k}}|^2+\frac{1}{4}t_{\perp}^2})$, with $d_{\mathbf{k}}=t[2\cos(\frac{\sqrt{3}}{2}k_y a)e^{-(i/2)k_x a}+e^{ik_x a}]$. Two of the bands are gapped (at $\mathbf{K},\mathbf{K}'$ by $t_{\perp}$) and become separated from the low-energy pair, which touches at $\mathbf{k}=0$ (see Fig. 1). The resulting density of states at zero energy is therefore finite.

The repulsive interaction $V(\mathbf{r}-\mathbf{r}')$ in Eq. (1) is taken to have a finite range ξ, which is much larger than the lattice spacing a. This is assumed to be the correct starting point since the full Coulomb interactions is screened[8] at low energy due to the finite density of states. Following Nilsson *et al.*,[9] we project out the gapped bands. The resulting low-energy effective (imaginary time) action (which includes both K and K' valleys) is

$$\mathcal{S}=\int d\tau d^2\mathbf{r}\left[\psi^{\dagger}\left(\frac{\partial}{\partial\tau}+\sum_{a=x,y}\Sigma^a d^a_{\mathbf{p}}\psi\right)\right]+\frac{1}{2}g_1\int d\tau d^2\mathbf{r}\psi^{\dagger}\psi(\mathbf{r},\tau)\psi^{\dagger}\psi(\mathbf{r},\tau)+\frac{1}{2}g_2\int d\tau d^2\mathbf{r}\psi^{\dagger}\Sigma^z\psi(\mathbf{r},\tau)\psi^{\dagger}\Sigma^z\psi(\mathbf{r},\tau)+\frac{1}{2}g_3\int d\tau d^2\mathbf{r}\sum_{a=x,y}\psi^{\dagger}\Sigma^a\psi(\mathbf{r},\tau)\psi^{\dagger}\Sigma^a\psi(\mathbf{r},\tau),\quad(3)$$

where the four component Fermi (Grassman) fields

$$\psi^{\dagger}(\mathbf{r},\tau)=\int_0^{\Lambda}\frac{d^2\mathbf{k}}{(2\pi)^2}e^{i\mathbf{k}\cdot\mathbf{r}}[a_1^{\dagger}(\mathbf{K}+\mathbf{k},\tau),b_2^{\dagger}(\mathbf{K}+\mathbf{k},\tau),a_1^{\dagger}(\mathbf{K}'+\mathbf{k},\tau),b_2^{\dagger}(\mathbf{K}'+\mathbf{k},\tau)]\quad(4)$$

and

$$d^x_{\mathbf{k}}=\frac{k_x^2-k_y^2}{2m},\quad d^y_{\mathbf{k}}=\frac{2k_xk_y}{2m},\quad \Sigma^x=1\sigma^x,\quad \Sigma^y=\tau^z\sigma^y,\quad \Sigma^z=\tau^z\sigma^z.\quad(5)$$

The Pauli matrices σ_j act on the layer indices 1–2 and the τ matrices act on the valley indices $\mathbf{K}$-$\mathbf{K}'$. The effective mass is $m=2t_{\perp}/(9t^2)$, and ψ represents $\frac{N}{2}$ copies of the four component pseudospinor. $N=4$ for spin 1/2, and, e.g., for $s=1,\ldots,N$, $\psi^{\dagger}\Sigma^z\psi(\mathbf{r},\tau)=\psi^{\dagger}_{\alpha s}\Sigma^z_{\alpha\beta}\psi_{\beta s}$. Note that Σ's have the same multiplication table as the Pauli σ's: $\Sigma^{\mu}\Sigma^{\nu}=1_4\delta_{\mu\nu}+i\epsilon_{\mu\nu\lambda}\Sigma^{\lambda}$ and are traceless too. Λ is a momentum cutoff, which restricts the modes to the vicinity of the $\mathbf{K}$-$\mathbf{K}'$ points and whose order of magnitude is $\lesssim\sqrt{2mt_{\perp}}$.

The coupling constant $g_1=\int d^2\mathbf{r}V(\mathbf{r})$, while g_2 and g_3 are zero in the starting action, but they get generated in the momentum-shell RG.[1] From simple power counting, the (engineering) scaling dimension of the field ψ is L^{-1} and L^2 for τ. This makes g_1, g_2, and g_3 marginal (at the tree-level) and the question is how they flow upon inclusion of the loop corrections. To answer this, we need to evaluate the diagrams in Fig. 2. The RG equations obtained by integrating fermion modes within a thin shell Λ and Λ/s (centered at the K point), and $\int_{-\infty}^{\infty}\frac{d\omega}{2\pi}$, are

$$\frac{dg_1}{d\ln s}=[-4g_1g_3]\frac{m}{4\pi},\quad(6)$$

$$\frac{dg_2}{d\ln s}=[-4(N-1)g_2^2+4g_3^2+4g_1g_2-12g_2g_3]\frac{m}{4\pi},\quad(7)$$

$$\frac{dg_3}{d\ln s}=[-(g_1-g_3)^2-(g_2-g_3)^2-2(N+1)g_3^2]\frac{m}{4\pi}.\quad(8)$$

We now analyze the qualitative nature of the above RG flows. Note that $\frac{dg_3}{d\ln s}\leq 0$ which means that, unless $g_1=g_2=g_3=0$ when the equality holds, g_3 strictly decreases under RG rescaling. We can therefore trade the parametric dependence on s of g_1 and g_2 for their dependence on g_3 and retain the direction of the RG flow. For $g_3<0(>0)$, an increase in $d\log s$ therefore corresponds to an increase (decrease) in $\frac{dg_3}{g_3}$. Since the system is autonomous, we can eliminate $\log s$ and arrive at a system

$$\frac{dg_1}{dg_3}=f\left(\frac{g_1}{g_3},\frac{g_2}{g_3}\right),\quad \frac{dg_2}{dg_3}=g\left(\frac{g_1}{g_3},\frac{g_2}{g_3}\right),\quad(9)$$

where

$$f(x,y)=\frac{-4x}{-x^2-y^2-2(N+2)+2x+2y},\quad(10)$$

$$g(x,y)=\frac{-4(N-1)y^2+4+4xy-12y}{-x^2-y^2-2(N+2)+2x+2y}.\quad(11)$$

The system of Eqs. (9)–(11) is in turn homogeneous and can therefore be written as

$$g_3\frac{d\frac{g_1}{g_3}}{dg_3}=-\frac{g_1}{g_3}+f\left(\frac{g_1}{g_3},\frac{g_2}{g_3}\right),\quad(12)$$

$$g_3\frac{d\frac{g_2}{g_3}}{dg_3}=-\frac{g_2}{g_3}+g\left(\frac{g_1}{g_3},\frac{g_2}{g_3}\right).\quad(13)$$

The above system has three fixed points, all of which have $g_1/g_3=0$, while $g_2/g_3=m_1,m_2,m_3$. As shown in Fig. 3, $m_1\approx-0.525$ and $m_3\approx 13.98$ are sinks, while $m_2\approx 0.545$ has one attractive direction and one repulsive. This means that once g_3 gets to be negative, only g_2 and g_3 become important

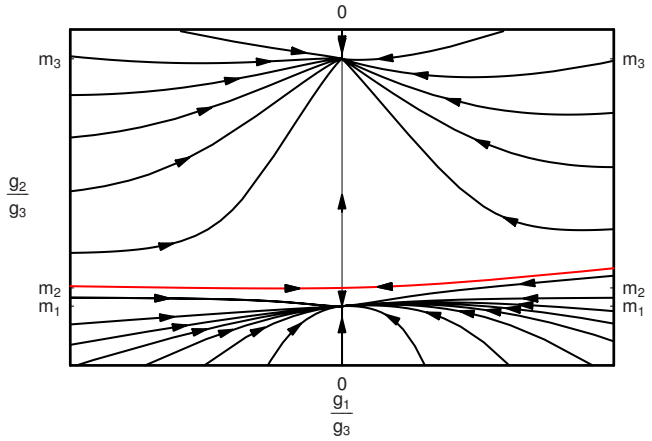

FIG. 3. (Color online) RG flow diagram of the ratios g_1/g_3 and g_2/g_3 for $g_3<0$. While the ratio g_1/g_3 flows to zero (even if the starting point is $g_2=g_3=0$ and $g_1\neq 0$), the ratio g_2/g_3 flows to a fixed value, indicating two stable and one unstable rays with slopes $m_1\approx -0.525$, $m_3\approx 13.98$, and $m_2\approx 0.545$, respectively.

(their ratio being fixed) while g_1 is too small compared to g_3. To see that this is indeed what happens if the starting point is $g_1(s=1)>0$ and $g_2(s=1)=g_3(s=1)=0$, note that Eqs. (6)–(8) imply that finite g_1 generates finite and negative g_3 upon first iteration, while g_2 remains zero until the second iteration. This means that we start with $g_1/g_3\to-\infty$ and $g_2/g_3=0$, which is *below* the (red) separatrix; thus, the flow is into the region of attraction of m_1 (Fig. 3).

From Eqs. (6)–(8), we see for the fixed ratios $g_1/g_3=0$ and $g_2/g_3=m_j$, g_3 becomes large and negative, indicating a runaway flow. Given the flow of g's, we can determine the susceptibilities toward the formation of ordered states. We consider coupling the fermions to external sources, which correspond to the possible broken-symmetry states and introduce additional terms in the action

$$\Delta\mathcal{S}=-\Delta_{ph}^{\mathcal{O}_i}\int d\tau d^2\mathbf{r}\,\psi^\dagger\mathcal{O}_i\psi(\mathbf{r},\tau)$$
$$-\Delta_{pp}^{\mathcal{O}_i}\int d\tau d^2\mathbf{r}\,\psi_{\alpha\sigma}\mathcal{O}^i_{\alpha\beta}\psi_{\beta\sigma'}(\mathbf{r},\tau). \quad (14)$$

Such terms, with infinitesimal Δ's explicitly break the symmetry. The question of instability is answered by finding the renormalization of the vertices.[10] The one with the strongest divergence determines the broken-symmetry state. After a straightforward calculation, we find that for a general particle-hole order parameter $\mathcal{O}_i=\tau^\mu\sigma^\nu$, where $\mu,\nu=0,1,2,3$ and $\tau_0=\sigma_0=1$,

$$\Delta_{ph,ren}^{\tau^\mu\sigma^\nu}=\Delta_{ph}^{\tau^\mu\sigma^\nu}\left(1+[Ag_1+Bg_2+Cg_3]\frac{m}{4\pi}\ln s\right), \quad (15)$$

where the coefficients A, B, and C are given in Table I. Similarly, for a general particle-particle order parameter $\psi_{\alpha\sigma}\mathcal{O}^{(i)}_{\alpha\beta}\psi_{\beta\sigma'}$,

TABLE I. (Upper half) The susceptibility coefficients A,B,C in Eq. (15) for different particle-hole order parameters $\psi^\dagger\mathcal{O}_i\psi$. In the physical case $N=4$. (Lower half) The susceptibility coefficients A',B',C' in Eq. (16) for different particle-particle order parameters $\psi_{\alpha\sigma}\mathcal{O}^{(i)}_{\alpha\beta}\psi_{\beta\sigma'}$.

$\psi^\dagger\tau^\mu\sigma^\nu\psi$	$\nu=0$	$\nu=x$	$\nu=y$	$\nu=z$
$\mu=0$	0,0,0	1,−1,−2N	1,−1,0	2,2,−4
$\mu=x$	1,−1,0	0,0,0	2,2,−4	1,−1,0
$\mu=y$	1,−1,0	0,0,0	2,2,−4	1,−1,0
$\mu=z$	0,0,0	1,−1,0	1,−1,−2N	2,2−4N,−4
$\psi_{\alpha s}(\tau^\mu\sigma^\nu)_{\alpha\beta}\psi_{\beta s'}$				
$\mu=0$	−1,−1,0	−2,2,−4	0,0,0	−1,−1,0
$\mu=x$	−2,2,−4	−1,−1,0	−1,−1,0	0,0,0
$\mu=y$	−2,2,−4	−1,−1,0	−1,−1,0	0,0,0
$\mu=z$	−1,−1,0	−2,2,−4	0,0,0	−1,−1,0

$$\Delta_{pp,ren}^{\tau^\mu\sigma^\nu}=\Delta_{pp}^{\tau^\mu\sigma^\nu}\left(1+[A'g_1+B'g_2+C'g_3]\frac{m}{4\pi}\ln s\right), \quad (16)$$

where the coefficients A', B', and C' are given in Table I.

The instability toward a particular order occurs at an energy scale (i.e., temperature) at which the corresponding coefficient of the $\ln s$ in Eqs. (15) and (16) diverges. Since $N=4$ and the fixed-point value of $g_2/g_3\approx -0.525$, with g_3 large and negative, it can be seen from Table I that the instability appears in the $\Sigma^{x,y}$ channel, which as we discuss next corresponds to a *nematic* order. The numerical integration of the RG equations (6)–(8), starting with $g_1(s=1)>0$ and $g_2(s=1)=g_3(s=1)=0$ shown in Fig. 4, indeed confirms that the susceptibility diverges fastest in this channel. Within the continuum model and in weak coupling, the instability is therefore toward the order parameter, which we can parametrize by a complex field

$$\Delta_{nem}(\mathbf{r})\equiv\Delta_x(\mathbf{r})+i\Delta_y(\mathbf{r})=\langle\psi^\dagger(\mathbf{r})(\Sigma^x+i\Sigma^y)\psi(\mathbf{r})\rangle.$$

To see that this is indeed a nematic order, note that at $\mathbf{q}=0$, it is both translationally invariant and even under rota-

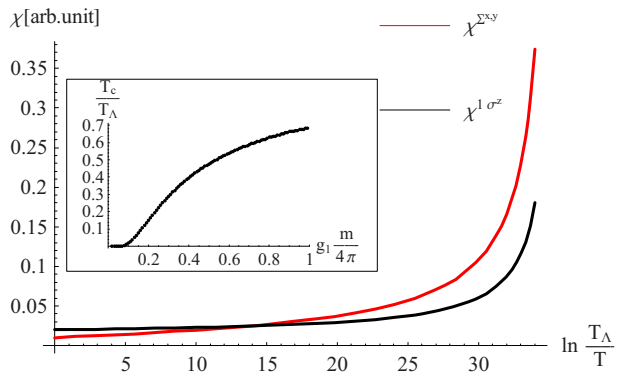

FIG. 4. (Color online) Numerical integration of the susceptibilities in Eq. (15) for $g_1(s=1)=0.01$ and $g_2(s=1)=g_3(s=1)=0$. The strongest divergence is toward the nematic order. (Inset) Numerically determined nematic transition temperature in units of cutoff $T_\Lambda\lesssim t_\perp$ as a function of the dimensionless coupling $g_1\frac{m}{4\pi}$.

tions by π. In fact, as the low-energy Hamiltonian is invariant under arbitrary rotations by an angle α, i.e., $U^{\dagger}(\alpha)\mathcal{H}U(\alpha)=\mathcal{H}$, where $U_{\alpha}=e^{-i\alpha\hat{L}_z}e^{-i\alpha\Sigma^z}$, $L_z=x\frac{\partial}{\partial y}-y\frac{\partial}{\partial x}$, we find that under a rotation by α

$$\Delta_{nem}(\mathbf{r}) \to \Delta_{nem}(\mathbf{r})e^{2i\alpha}.$$

This shows that the order parameter is even under rotations by π and odd under rotations by $\pi/2$, which makes it nematic. For uniform $\Delta_{nem}(\mathbf{r})$, the quadratic degeneracy point is split into two (massless) Dirac points by an amount proportional to the magnitude of the order parameter and the direction given by the nematic director.

The underlying lattice further breaks the full rotational symmetry of the effective Hamiltonian down to hexagonal symmetry centered on a_2-b_1 site, where the standard operations of C_{6v} must be accompanied by the appropriate layer permutations. The two components of the order parameter, which give finite expectation values of, for instance,

$$\Delta_x(\mathbf{r}) = \left\langle a^{\dagger}_{1\sigma}(\mathbf{r})\left[b_{2\sigma}(\mathbf{r}-a\hat{x}) - \frac{1}{2}\sum_{s=\pm} b_{2\sigma}\left(\mathbf{r}+\frac{a}{2}\hat{x}+s\frac{\sqrt{3}}{2}\hat{y}\right)\right] + \text{H.c.}\right\rangle, \tag{17}$$

and

$$\Delta_y(\mathbf{r}) = \left\langle a^{\dagger}_{1\sigma}(\mathbf{r})\left[\frac{\sqrt{3}}{2}\sum_{s=\pm} s b_{2\sigma}\left(\mathbf{r}+\frac{a}{2}\hat{x}+s\frac{\sqrt{3}}{2}\hat{y}\right)\right] + \text{H.c.}\right\rangle, \tag{18}$$

form a two-dimensional representation of the hexagonal group. Note that the nematic order parameter remains even under π rotation followed by the layer permutation.

We expect that the lattice has an important effect on the critical nature of the phase transition, which would otherwise be of Kosterlitz-Thousless kind. The reason is the existence of the third-order invariant $\Delta_x^3-3\Delta_x\Delta_y^2$. As a result, the finite temperature phase transition should be described by the effective Hamiltonian

$$\mathcal{H}_{nem} = \sum_{\langle \mathbf{x}\mathbf{x}'\rangle} -J\cos\{2[\theta(\mathbf{x})-\theta(\mathbf{x}')]\} + h\sum_{\mathbf{x}}\cos[6\theta(\mathbf{x})], \tag{19}$$

where $\Delta_x(\mathbf{x})+i\Delta_y(\mathbf{x})=e^{2i\theta(\mathbf{x})}$, $\theta\in(0,2\pi]$, and the sum runs over the vertices of the triangular sublattice spanned by a_1 sites. This corresponds to the $p=3$ case of the two-dimensional planar model studied by José *et al.*[11] and the concomitant absence of the Gaussian spin-wave phase. Instead, there is a continuous transition between the low-temperature phase, where the director locks into one of three values, and a high-temperature phase, where vortices unbind. Such transition is believed to belong to the two-dimensional three-state Potts model universality class[12] with exponents[13] $\nu=5/6$ and $\eta=4/15$.

Finally, we discuss the effects of the trigonal warping, which splits each of the quadratic degeneracies into four massless Dirac points, which were ignored up to now. If we denote the energy scale associated with such terms as T_{trig}, below which the dispersion must be modified, then the transition will still occur provided that the mean-field transition temperature T_c estimated from the above model and plotted in the inset of Fig. 4 satisfies $T_c \gg T_{trig}$. For screened Coulomb interactions[8] $g_1\frac{m}{4\pi}\sim\mathcal{O}(1)$, leading to $T_c \lesssim t_{\perp}$. Since the current estimates of T_{trig} are of the same order of magnitude,[14] the ultimate test is experimental.

Recently, we became aware of Ref. 15 where lattices with fourfold and sixfold rotational symmetries are constructed with the parabolic degeneracy points protected by the point-group symmetry. In there, the degeneracy point maps unto itself under time reversal, unlike our K and K'. Within mean-field approximation, the nematic was also found.

Note added in proof. Recently, other papers that discuss related material have appeared.[16,17]

This work is supported in part by NSF Grant No. DMR-0704133 (K.Y.). Part of this work was carried out while the authors were visiting Kavli Institute for Theoretical Physics (KITP). The work at KITP is supported in part by NSF Grant No. PHY-0551164.

[1] R. Shankar, Rev. Mod. Phys. **66**, 129 (1994).
[2] K. S. Novoselov, E. McCann, S. V. Morozov, V. I. Fal'ko, M. I. Katsnelson, U. Zeitler, D. Jiang, F. Schedin, and A. K. Geim, Nat. Phys. **2**, 177 (2006).
[3] E. McCann and V. I. Fal'ko, Phys. Rev. Lett. **96**, 086805 (2006).
[4] A. H. Castro Neto, F. Guinea, N. M. R. Peres, K. S. Novoselov, and A. K. Geim, Rev. Mod. Phys. **81**, 109 (2009).
[5] A. K. Geim and A. H. MacDonald, Phys. Today **60**(8), 35 (2007).
[6] J. Nilsson, A. H. Castro Neto, N. M. R. Peres, and F. Guinea, Phys. Rev. B **73**, 214418 (2006).
[7] H. Min, G. Borghi, M. Polini, and A. H. MacDonald, Phys. Rev. B **77**, 041407(R) (2008).
[8] E. H. Hwang and S. Das Sarma, Phys. Rev. Lett. **101**, 156802 (2008).
[9] J. Nilsson, A. H. Castro Neto, F. Guinea, and N. M. R. Peres, Phys. Rev. B **78**, 045405 (2008).
[10] A. Chubukov, arXiv:0902.4188, Physica C (to be published).
[11] J. V. José, L. P. Kadanoff, S. Kirkpatrick, and D. R. Nelson, Phys. Rev. B **16**, 1217 (1977).
[12] D. R. Nelson, *Defects and Geometry in Condensed Matter Physics* (Cambridge University Press, Cambridge, UK, 2002), p. 56.
[13] F. Y. Wu, Rev. Mod. Phys. **54**, 235 (1982).
[14] L. M. Zhang, Z. Q. Li, D. N. Basov, M. M. Fogler, Z. Hao, and M. C. Martin, Phys. Rev. B **78**, 235408 (2008).
[15] K. Sun, H. Yao, E. Fradkin, and S. A. Kivelson, Phys. Rev. Lett. **103**, 046811 (2009).
[16] F. Zhang, H. Min, M. Polini, and A. H. MacDonald, Phys. Rev. B **81**, 041402 (2010).
[17] R. Nandkishore and L. Levitov, arXiv:0907.5395 (unpublished).